

# Supporting Information for Chronoamperometric Study of Conformational Relaxation in PPy(DBS)

B. Jason West, Toribio F. Otero, Benjamin Shapiro, and Elisabeth Smela

## 1 JUSTIFICATION OF RESULTS

### 1.1 Effect of the Working Electrode Surface

The effect of the working electrode surface must be considered in this type of study, since it is thought to strongly influence the kinetics of relaxation [1]. The ESCR model was developed based on experimental data obtained from PPy films deposited on polished Pt. In those (anion-transporting) systems, nucleation was observed in the form of expanding cylinders that coalesced over time (visible via the electrochromism of these polymers). The ESCR model thus included the effects of nucleation and coalescence. This is in contrast to the uniform color changes during switching in our study, which employed as substrates thermally evaporated Au on highly polished Si (see Figure 1-SI): no nucleation occurred (or, conversely, nucleation occurred in so many places at once that it could not be observed). So, while our results agree with the ESCR model, it should be noted that future work should adapt the model to include uniform front propagation. Future models should also include the role of drift on ion transport.

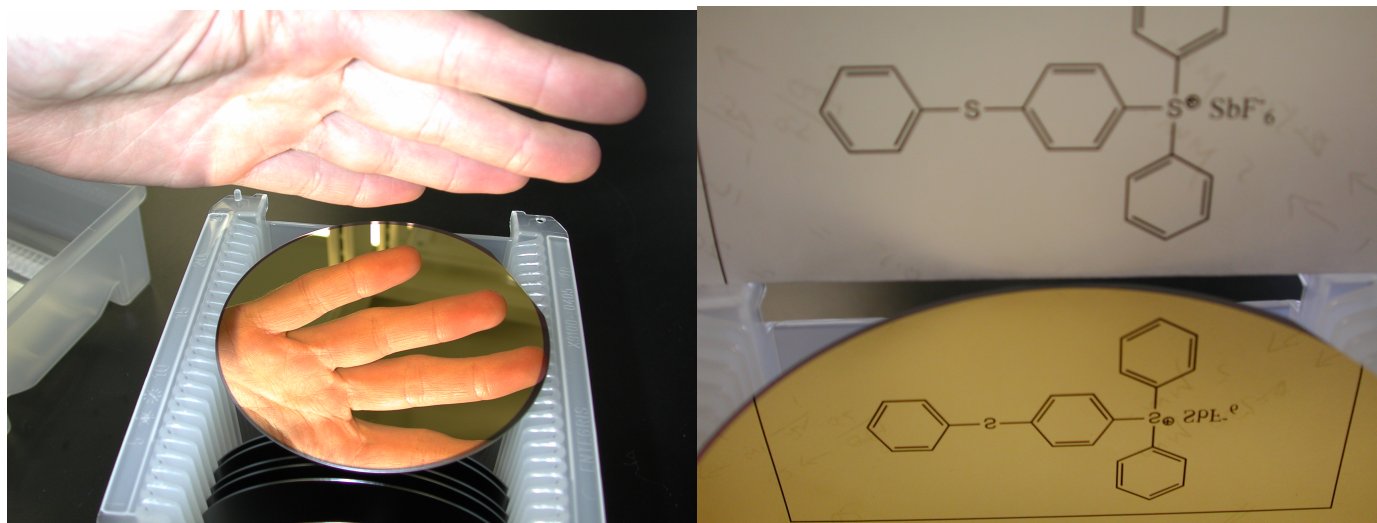


**Figure 1-SI. Photographs of the mirror-like surface of a representative Au-covered, oxidized Si wafer that was used in the study.**

### 1.2 Effect of Thickness

The PPy thickness was also of importance in determining the results of this study. Since the films were fairly thick (5000 Å), ion transport occurred simultaneously both in the in-plane and the out-of-plane directions, again observed via the electrochromism of the films. (This is typical for PPy(DBS).) This complicates data analysis, since both ion mobility and conformational relaxation could be different in the two directions. Future work involving films of varying thickness and area showing how the cathodic

current shoulder evolves would help to explain the role that conformational relaxation plays in ion transport in the two directions.

### 1.3 Exponential Curve Fits

The use of exponential functions to fit the CA data, rather than a  $t^{-1/2}$  relationship as is usually used in electrochemistry (the Cottrell equation), may have been surprising to some readers. It is important to recall that the Cottrell expression is based on the diffusion of species in a liquid electrolyte to the surface of a solid electrode; it does not take into account migration (movement of charge under electric fields), nor does it take into account species moving through a polymer matrix. The stretched exponential function has been used to empirically describe a range of physical properties in complex systems such as polymers and glasses [2-4]. It can also be used to fit a distribution of diffusion times in swelling/shrinking polymers. The distribution of times is thought to arise from local variations in the diffusion coefficients within the polymer due to local differences in oxidation level, swelling, crosslinking, chain stiffness, etc. Just as defects and crosslinking produce a distribution of oxidation and reduction potentials, and thus broad peaks in the cyclic voltammograms compared to those obtained for electrochemical reactions at liquid/solid interfaces, these parameters would be expected to affect the scattering of ions, and thereby the diffusion coefficient. The movement of ions through a dense polymer electrode whose properties (oxidation level, volume, chain stiffness, solvation) are changing simultaneously with the arrival or departure of those very ions, makes this redox a complex process. It is further complicated by the fact that migration cannot be neglected [5,6]. Furthermore, as shown by these and prior papers on ESCR processes, the rate limiting step may not be diffusion at all, but may be changes in chain conformation. Therefore, one should not expect the Cottrell equation to apply.

## 2 CYCLIC VOLTAMMETRIC SCANS

Figure 2-SIa shows cyclic voltammograms taken periodically throughout a CA series on one sample, and Figure 2-SIb shows single scans from each of the three samples used in the study. As explained in section 2.1.3 of the main text, these scans were recorded in order to ascertain the state of the films following each set of CA steps. Figure 2-SIa shows that there was relatively little change between cycles, which means that the samples did not significantly delaminate or degrade during the course of the study. Figure 2-SIb shows that the reduction and oxidation peaks occurred at the same potentials for each sample used in the study, showing that the results from each sample are comparable. (The variation in charge from sample to sample is due variation in the width of the samples (they varied by ~ 1 mm) and the immersed depth of the samples (which also varied by ~ 1 mm).)

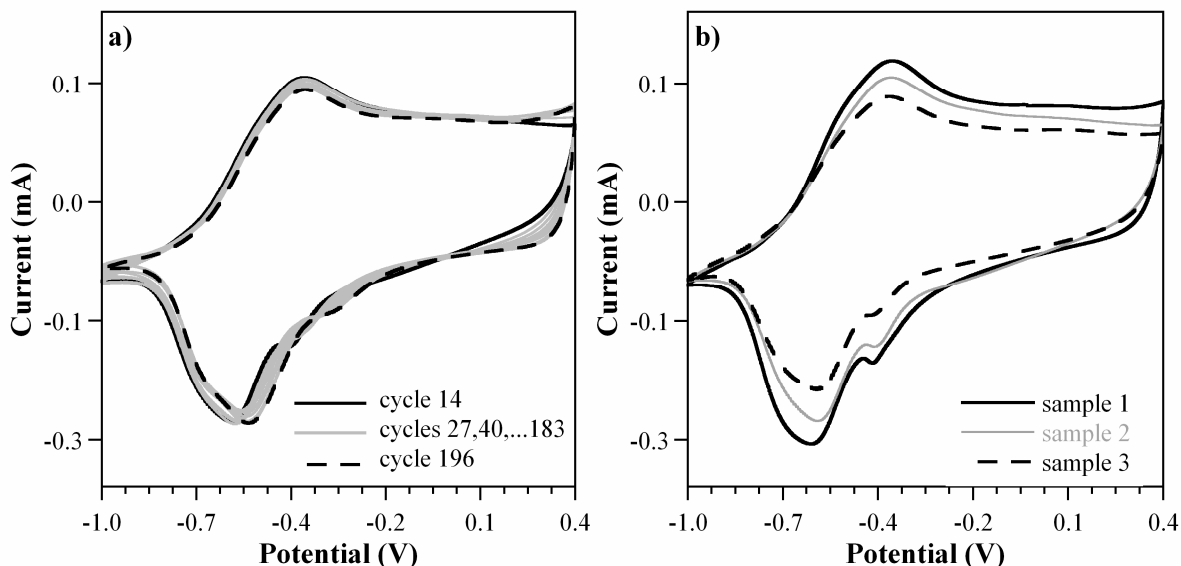


**Figure 2-SI.** Cyclic voltammograms of a) 13-CA-cycle increments up to 196 cycles on one sample, and b) single cycles from all three samples used in the study.

### 3 ANODIC CHARGE CONSUMED DURING CHRONOAMPEROMETRY

The charge consumed during the anodic step,  $Q_{an}$ , was calculated by integrating the area under the current-corrected CA curve between 0 and 5 seconds. Figure 3-SI shows  $Q_{an}$  as a function of  $E_{an}$  and  $E_{ca}$ . When stepping from cathodic potentials that lie below the peak for the reduction process in the PPy(DBS), i.e.,  $E_{ca} \leq -1$  V (upper curves in Figure 3-SIa), the charge increased essentially linearly with  $E_{an}$ , consistent with the constant pseudo-capacitive current in the CVs above -0.15 V. Furthermore, the curves overlay each other. This means that increasing the cathodic potential does not change the amount of charge consumed by the subsequent oxidation. This range of potentials will be referred to as “regime II”.

When stepping from less cathodic potentials,  $E_{ca} > -1$  V (lower curves in Figure 3-SIa), the charge increased less rapidly with  $E_{an}$ , and the charge depended on  $E_{ca}$ . This range of potentials will be called “regime I”. In regime I, the reduction level of the polymer depends on  $E_{ca}$ , whereas in regime II the polymer is fully reduced, and cannot be further reduced by increasing  $E_{ca}$ . The same data are plotted as a function of  $E_{ca}$  in Figure 3-SIb, where the two regimes are evident. There was a discontinuity between -0.95 and -1.00 in all the data, the reason for which is unclear.

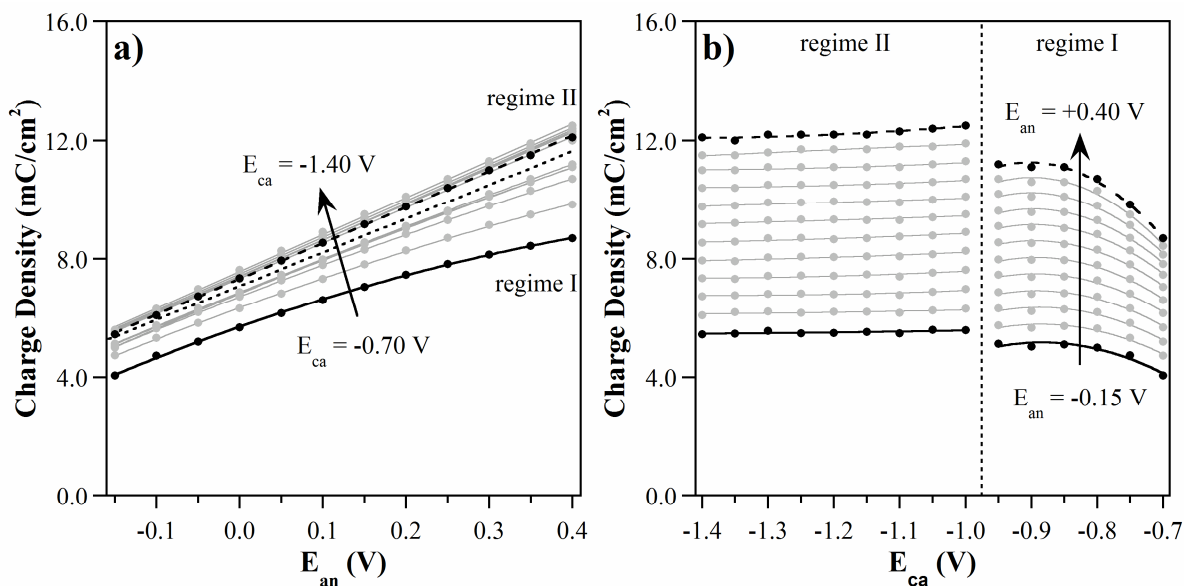


**Figure 3-SI. Anodic charge as a function of a) anodic potential for different initial cathodic potentials and b) cathodic potential for different anodic potentials. The measured values are indicated by points; the lines are a guide to the eye. The dotted line separates the curves in regimes I and II.**

## 4 CATHODIC CURRENTS DURING CHRONOAMPEROMETRY

### 4.1 Role of Cathodic Potential

The evolution of the cathodic CAs with increasingly cathodic potential  $E_{ca}$ , from -0.7 to -1.4 V, is shown in Figure 5-SIa, and corresponds to data in Figures 4 and 12 in the main text. The two-regime behavior was observed on all three samples. Exponential curve fits and the resulting ESCR peaks are shown in Figure 5a) and b).

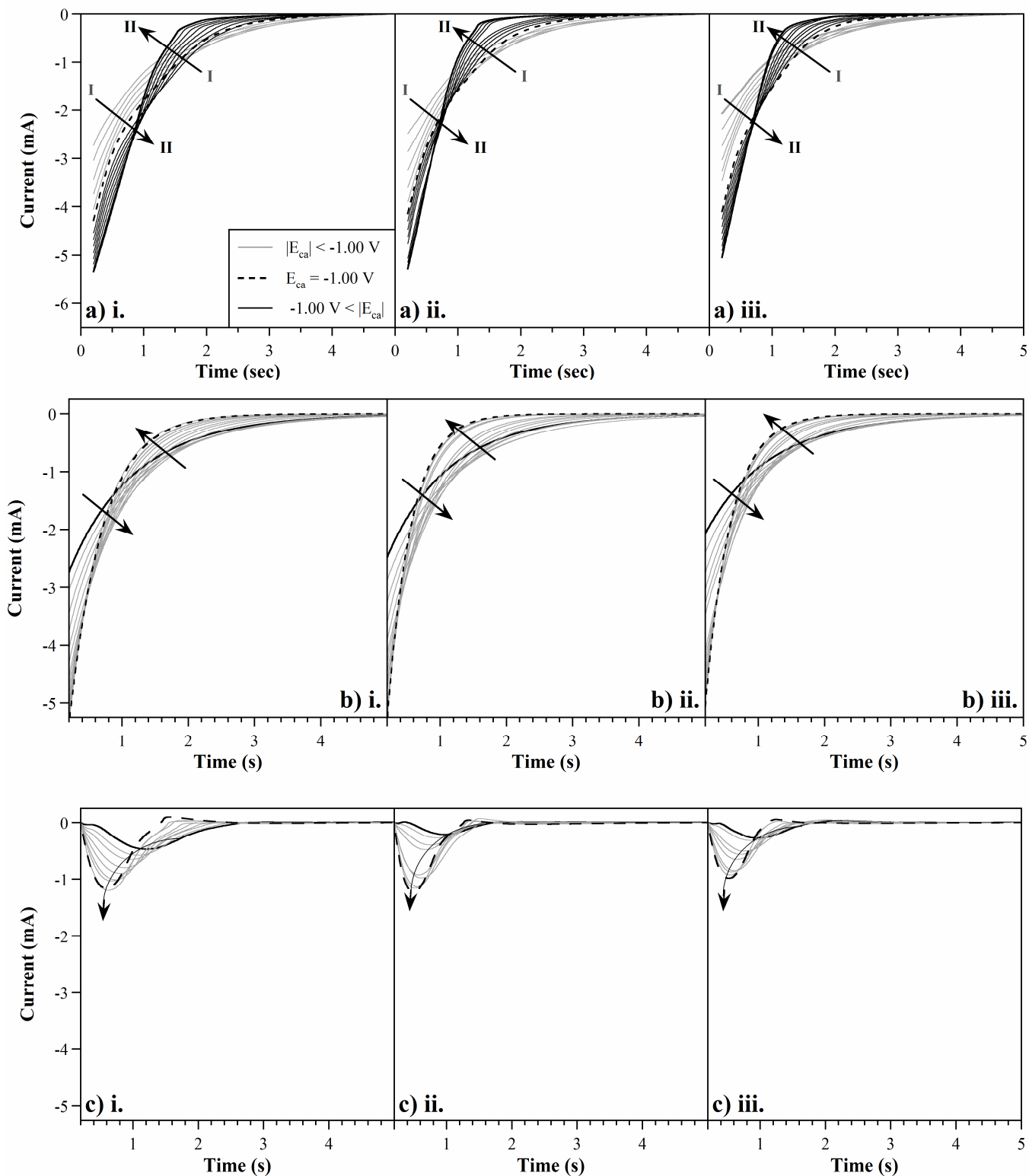


**Figure 5-SI.** a) Cathodic currents , b) exponential and c) ESCR components of cathodic curve fits for increasingly cathodic initial potentials from an initial  $E_{an}=+0.40$ V. Data from the three studied samples are denoted by roman numerals.

Figure 6-SI (also corresponding to Figure 12 in the main text) shows cathodic curve fits for a single pre-applied  $E_{an}$  (+0.40 V), stepping to three successively higher cathodic potentials  $E_{ca}$ . These fits are shown primarily to illustrate the point at which  $I_1$ , (recall that  $I_1$  and  $I_2$  are the regions of the CA

curves in which the curve fitting error was calculated) shrank to zero. This point was estimated to be  $-1.05$  V; please note that at  $-1.00$  V, there is still a small delay on the ESCR peak, corresponding to a small region of the CA curve which was fit with the exponential.

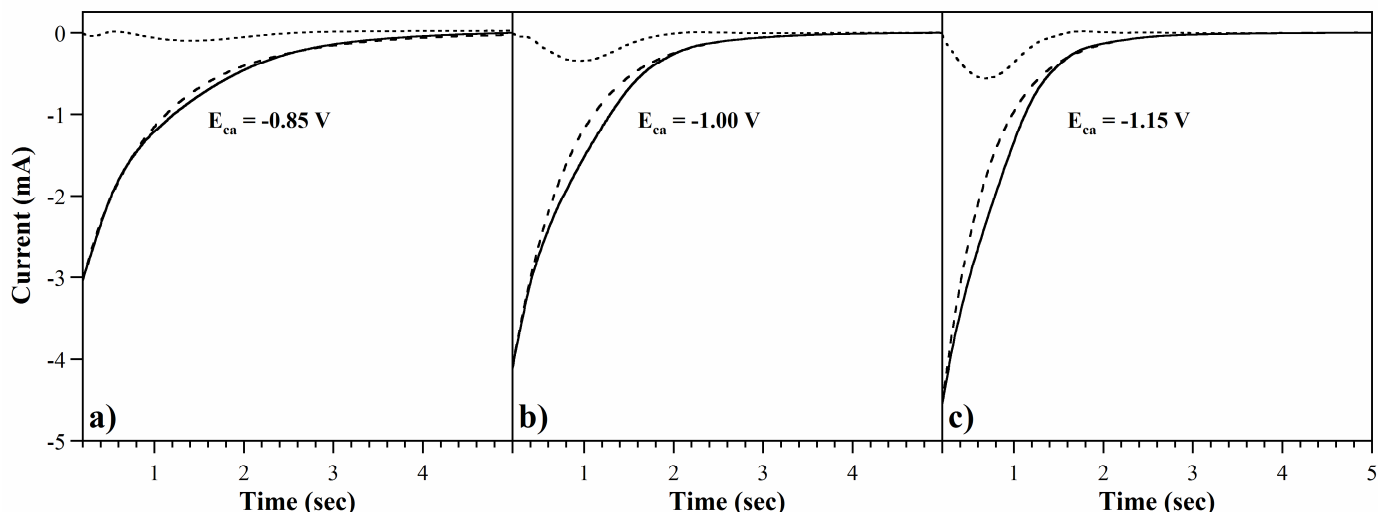


**Figure 6-SI.** a) CA data (solid curves), exponential fits (dashed lines), and subtracted (ESCR) components (dotted lines) for  $E_{ca} = -0.85$  V, stepping from  $E_{an} = +0.40$  V. b) fitted curves for  $E_{ca} = -1.00$  V. c) fitted curves for  $E_{ca} = -1.15$  V.

#### 4.1.1.1 Time Dependence: Exponential Curve

In Figure 7-SI (corresponding to Figure 13 in the main text), the natural log of the cathodic exponential time constant,  $\ln(\tau_{exp})$ , is plotted as a function of  $E_{ca}$  for the three samples. Small differences were observed, but the trend was the same for all of the samples.

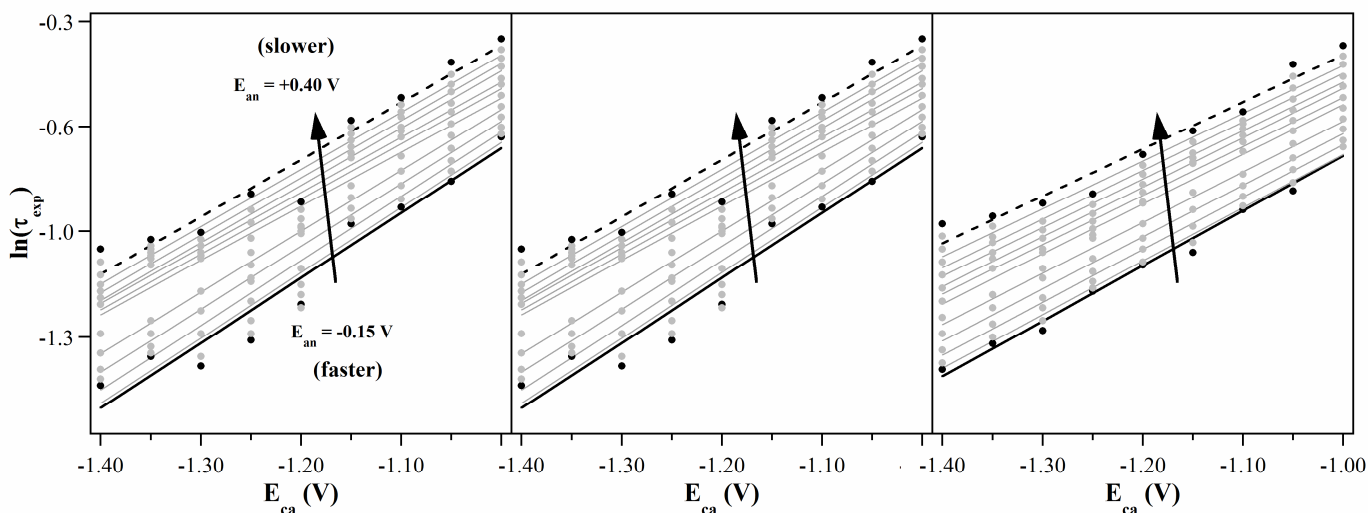


**Figure 7-SI.** Natural logarithm of the time constants for the exponential curve fits to the tails of the cathodic CAs, plotted as a function of cathodic potential upon stepping from different pre-applied anodic potentials (the lines are a guide to the eye).

#### 4.1.1.2 *Time Dependence: ESCR Peak*

Figure 8-SI (which corresponds to Figure 14 in the main text) shows the ESCR peak position in time,  $\tau_{ESCR}$ , as a function of  $E_{ca}$  for the three samples.

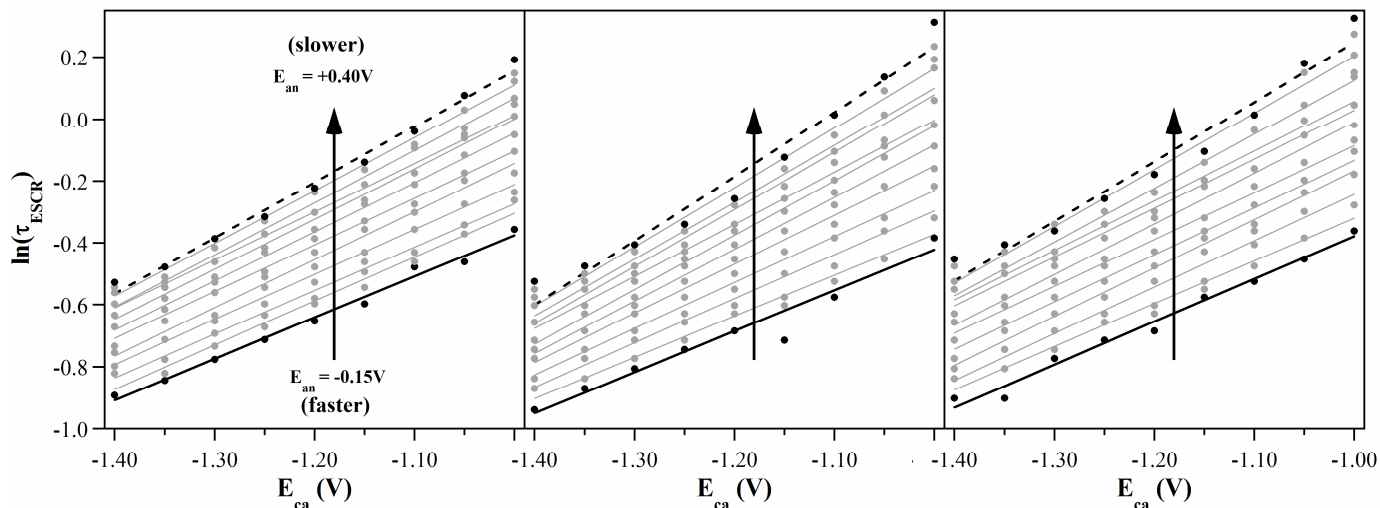


**Figure 8-SI. Natural logarithm of the time constants for the subtracted (ESCR) curves, plotted as a function of cathodic potential upon stepping from different pre-applied anodic potentials (lines).**

#### 4.1.1.3 *Charge*

The consumed cathodic charge,  $Q_{ca}$ , the charge in the fitted exponential,  $Q_{exp}$ , and the charge in the subtracted peak,  $Q_{ESCR}$ , are shown as a function of  $E_{ca}$  in Figure 9-SI (the consumed cathodic charge corresponds to Figure 10 in the main text).  $Q_{exp}$  decreases linearly with increasingly cathodic potentials for the entire range of anodic potentials. As expected,  $Q_{ESCR}$  experiences a corresponding increase with increasingly cathodic potentials to compensate for the leftover charge\*. The increase of  $Q_{ESCR}$  and the decrease of  $Q_{exp}$  with increasing cathodic potential are consistent with the ESCR model, assuming that the peak is related to conformational relaxation. Additionally,  $Q_{ESCR}$  and  $Q_{exp}$  correspond well with the charge densities and proportions of the two Gaussian peaks in the CVs (paper Figure 4b).

Note that the x-axes in a) extend to -0.7 V, but only to -1.0 V in b) and c), because only curve fits at  $E_{ca}$  more cathodic than -1.0 V were considered. Also note that the y-axes in a), which shows charge density, are different than those in b) and c), which show charge, and that b) and c) have different scales. The charges ( $Q_{ca}$  vs.  $Q_{exp}+Q_{ESCR}$ ) don't match up because the curve fitting was only done past 0.2 seconds, so the fitted charges only include those data.

\* Keep in mind that at this point in the data analysis, the original data have been: 1) corrected for baseline current at 5 s, 2) corrected for capacitive current below 0.2 s, 3) partially fit with exponential curves, and 4) the two components of the fitted curves have been integrated to obtain the charge in Figure 9-SI. With this many levels of processing, we do not intend to make exact statements about the data, especially with the ESCR peaks, which contain ~20% of the charge of the exponential peaks, and are thus ~5x more susceptible to noise in data processing. Rather, we present these data to show *general* trends that are nonetheless consistent across all three data sets and consistent with the ESCR model.

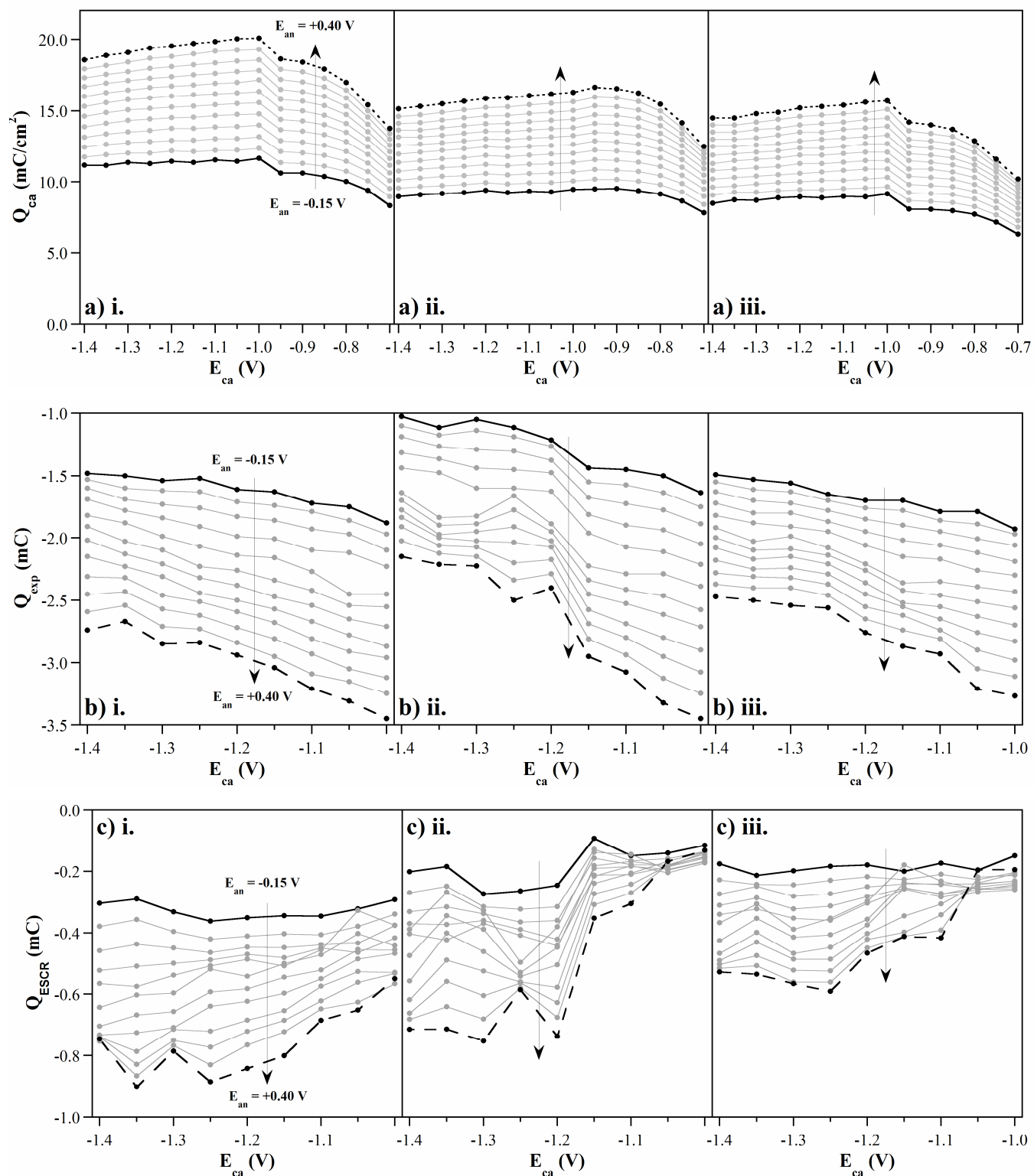


**Figure 9-SI.** Cathodic charge consumed during steps to various cathodic potentials, calculated from a) the original experimental data, b) the exponential fits, and c) the subtracted peak components as a function of  $E_{ca}$  for a series of initial  $E_{an}$ . Data from the three studied samples are denoted by roman numerals.

## 4.2 Role of Anodic Potential

Figure 10-SI shows cathodic CAs (row a), exponential curve fits (row b), and ESCR curves (row c) for a single  $E_{ca}$  (-1.40 V) vs.  $E_{an}$ . This plot corresponds to Figures 15 and 16 in the main text.

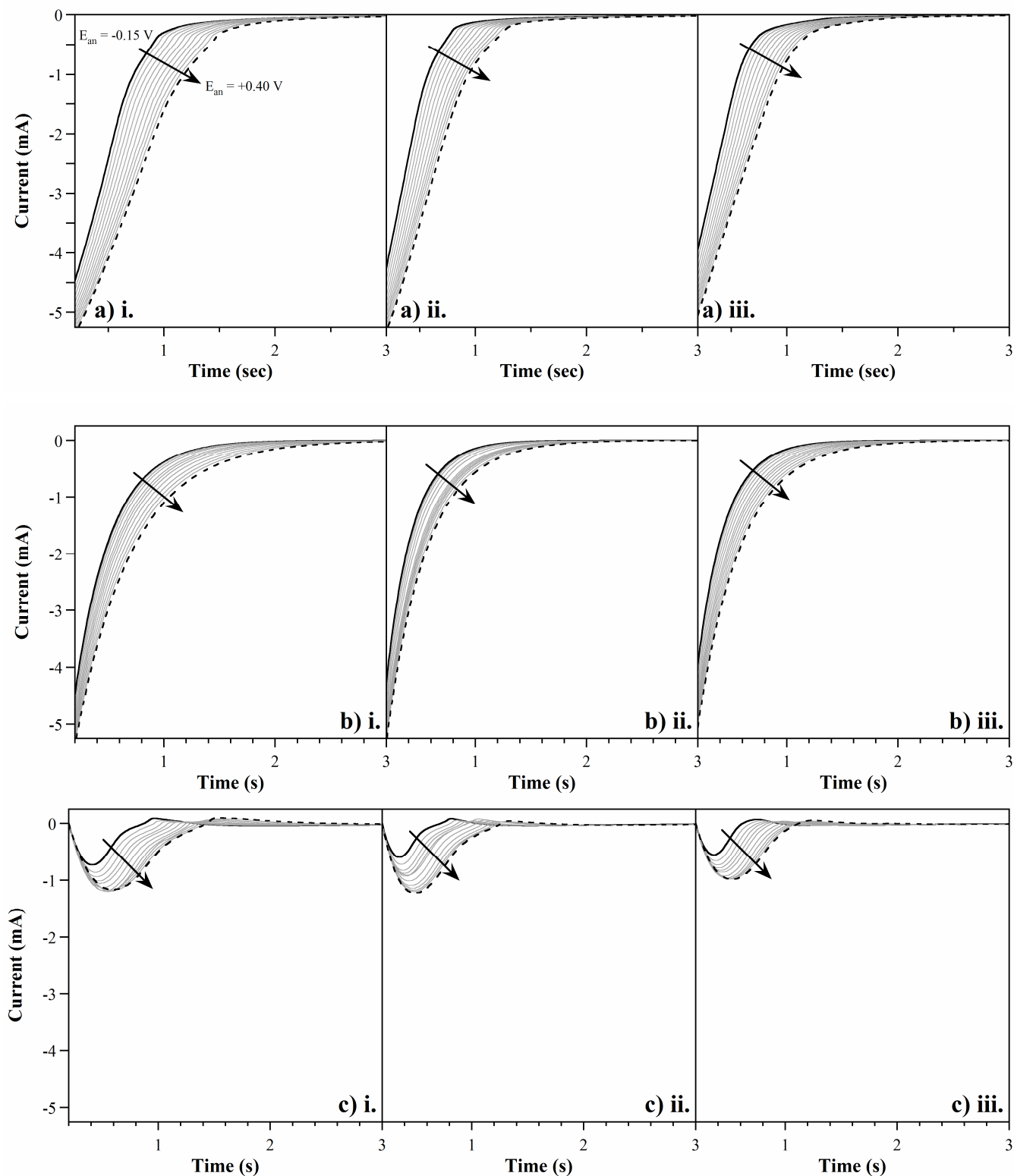


**Figure 10-SI.** a) Cathodic currents, b) exponential and c) ESCR components of cathodic curve fits for increasingly anodic initial potentials from an initial  $E_{ca} = -1.40$  V. Data from the three studied samples are denoted by roman numerals.

#### 4.2.1.1 Time Dependence: Exponential Curve

Figure 11-SI (corresponding to Figure 17 in the main text) shows the dependence of  $\ln(\tau_{exp})$  on  $E_{an}$ . Results were again consistent for the three samples.

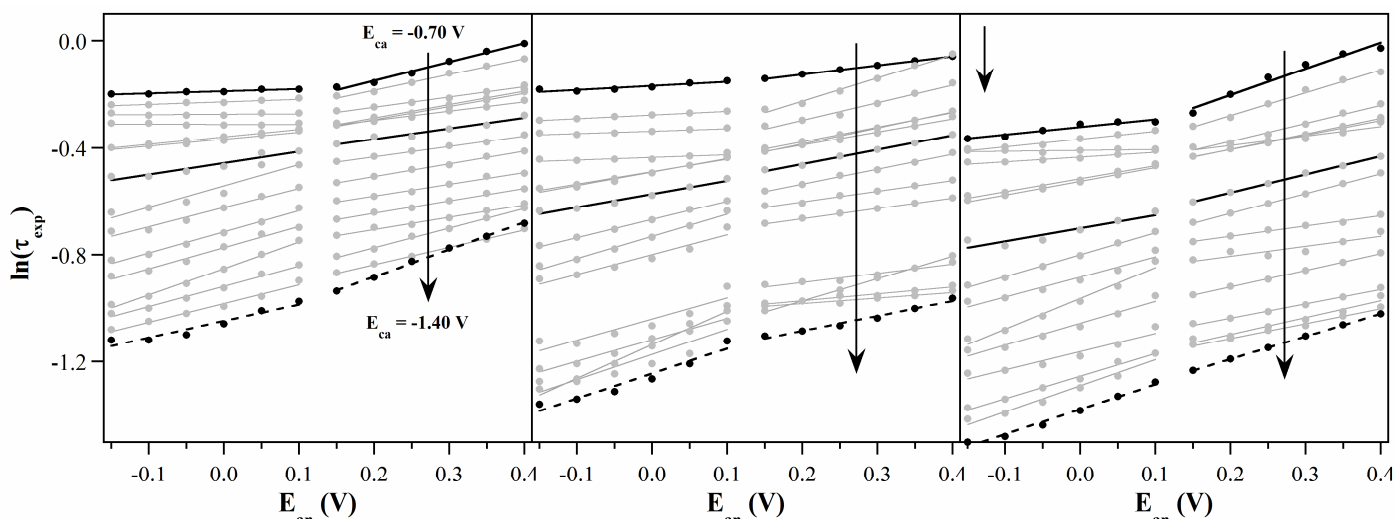


**Figure 11-SI.** Cathodic exponential time constants as a function of the pre-applied anodic potential upon stepping to different cathodic potentials.

#### 4.2.1.2 Time Dependence: ESCR Peak

ESCR peak times  $\tau_{ESCR}$  are plotted vs.  $E_{an}$  in Figure 12-SI (corresponding to Figure 18 in the main text). Results were consistent across all samples.

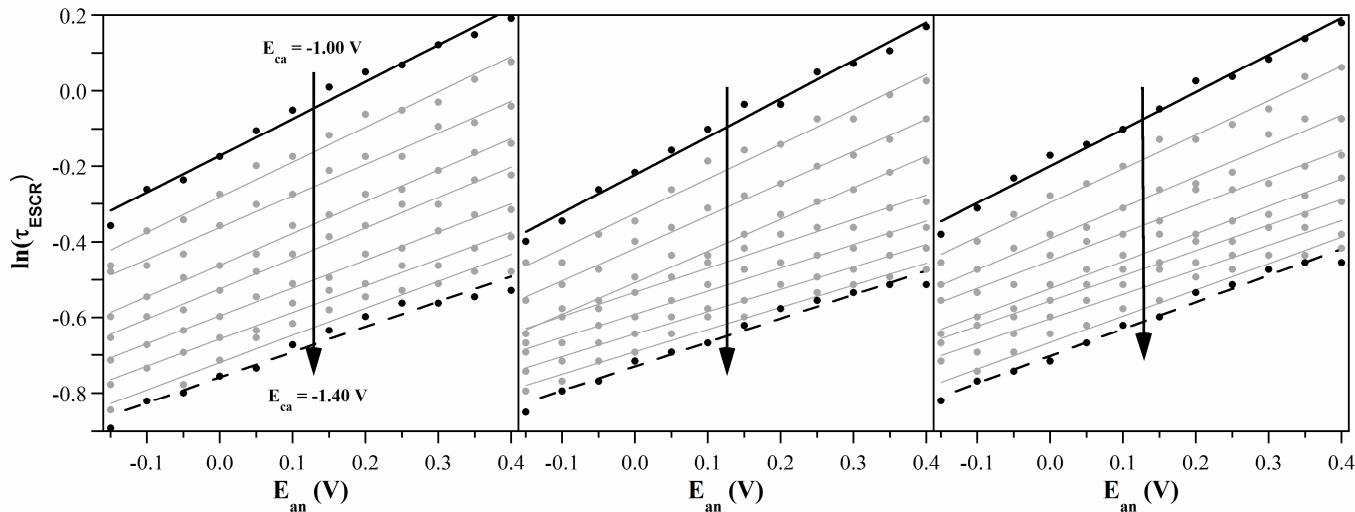


**Figure 12-SI.** Natural log of the ESCR peak time as a function of pre-applied anodic potential. QPC

## 4.2.2 Charge

Analogously to Figure 9-SI, which examined the consumed cathodic charge as a function of cathodic potential, Figure 13-SI shows the cathodic charge, exponential charge, and ESCR peak charge as a function of the applied anodic potential. There is no corresponding plot in the main text. Consistency was observed for all samples.

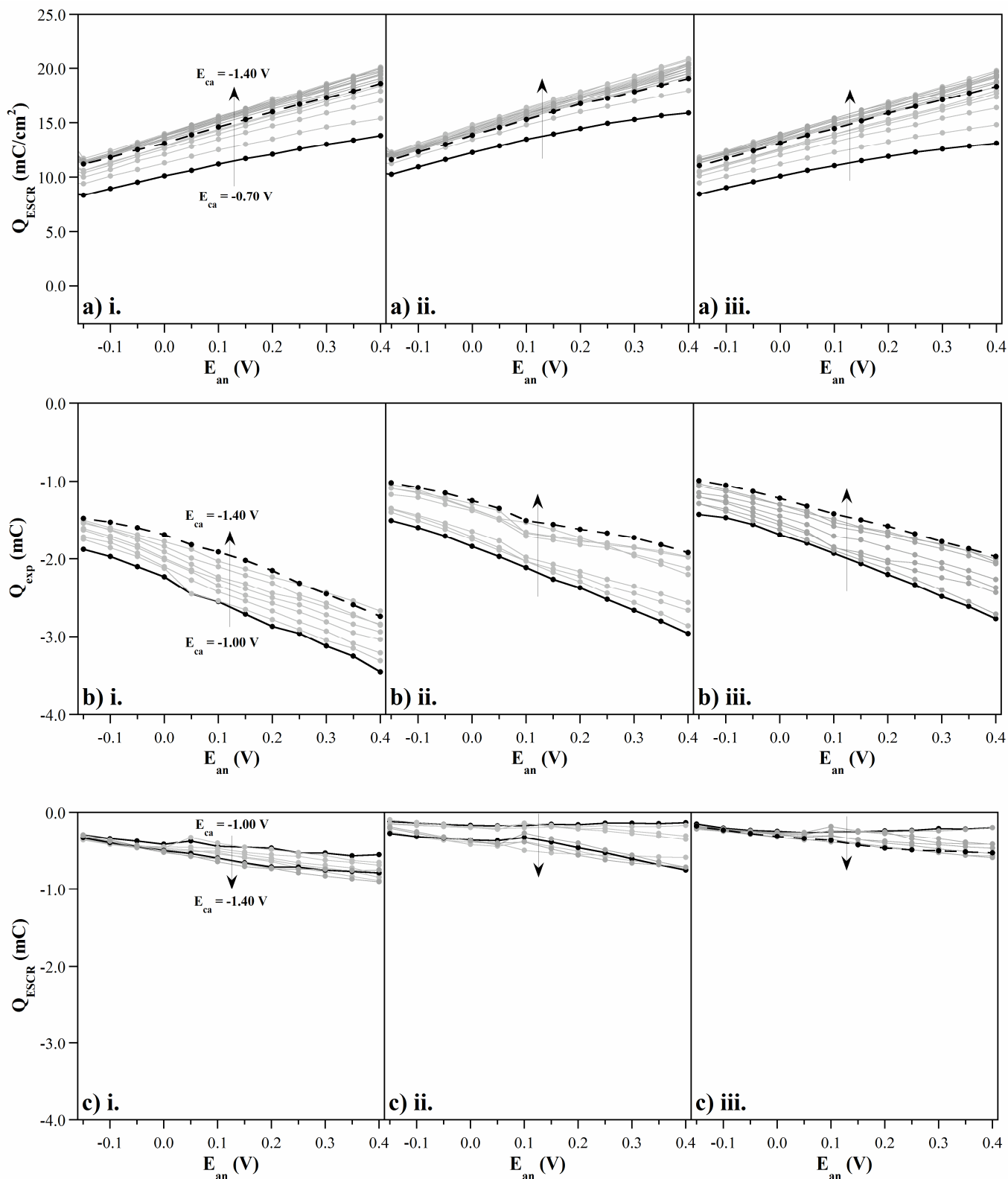


**Figure 13-SI. Cathodic charge consumed during steps to different anodic potentials, calculated from a) the original experimental data, b) the exponential fits, and c) the subtracted peak components as a function of  $E_{an}$  for a series of initial  $E_{ca}$  (-1.40 V). Data from the three studied samples are denoted by roman numerals. Note that the y-axes in a), which shows charge density, are different than those in b) and c), which show charge.**

## 5 CONFORMATIONAL ENERGIES $z_c$ AND $z_r$ IN VARIOUS POLYMERS

The values of the conformational energies  $z_c$  and  $z_r$  found in this work are compared with the values reported for other systems in Table I-SI and Figure 14-SI. In anion-transporting polypyrroles, the values of  $z_c$  and  $z_r$  are generally larger than those in PPy(DBS). However, it is important to note that these numbers cannot be directly compared because the film thicknesses were different, and film thickness affects these values since the molecular structure changes as a function of polymerization time. In addition, in order to use these values in a comparative way, a material reference is required, i.e. the charge consumed per unit of PPy mass during a voltammetric step to the same anodic over-potential.

**Table I-SI. Values of the conformational energies in various systems.**

Polymer	Solvent	Salt	$z_c$ (kC/mol)	$z_r$ (kC/mol)	$\Delta H^*$ (kJ/mol)	$\Delta H$ (kJ/mol)	Reference
<b>Cation-Transporting Polypyrroles</b>							
PPy(DBS)	water	NaDBS	1.5–2.6	2.8-4.5			this work
PPy(pTS)	PC	LiClO <sub>4</sub>	2.4				[7]
<b>Anion-Transporting Polypyrroles</b>							
PPy	ACN	LiClO <sub>4</sub>	4.2	7.4			[8]
PPy	ACN	LiClO <sub>4</sub>	3.5			28	[9]
PPy	ACN	LiClO <sub>4</sub>	5.6	2.7			[10]
PPy	PC	LiF, LiCl, LiI, LiBr	2.2				[11]
PPy	PC	LiClO <sub>4</sub>	3.2-5.2 <sup>††</sup>				[12]
PPy	PC	LiClO <sub>4</sub>	2.5	6.0	21.3		[13]
PPy	PC	LiClO <sub>4</sub>	4.6	4.4-7.7 <sup>†</sup>			[14]
PPy	PC	LiClO <sub>4</sub>	4.4	5.4	28		[15]
PPy\dc\n (	PC	LiClO <sub>4</sub>	4.1	6.0			[10]
PPy	sulfolane	LiClO <sub>4</sub>	3.1	9.0			[10]
PPy	acetone	LiClO <sub>4</sub>	3.6	8.0			[10]
PPy	DMSO	LiClO <sub>4</sub>	4.5	4.7			[10]
PPy	water	LiClO <sub>4</sub>				27	[16]
<b>Anion-Transporting Polyaniline</b>							
PANI	ACN	LiClO <sub>4</sub>	5.5	3.5-9.6 <sup>†</sup> from text 4.7-11.7 <sup>†</sup> from graph	14		[17]
PANI	ACN	LiClO <sub>4</sub>	5.5			14	[9]
<b>Different Anion-Transporting Polymers</b>							
poly(1-methyl pyrrole)	ACN	LiClO <sub>4</sub>	4.4			17	[9]
poly(methyl-aniline)	ACN	LiClO <sub>4</sub>	6.9			10	[9]
poly(thiophene)	ACN	LiClO <sub>4</sub>	2.7			24	[9]
poly(3-methylthiophene)	ACN	LiClO <sub>4</sub>	3.5			16	[9]

<sup>†</sup> The coefficient  $z_r$  depends on the pre-applied compaction potential.

<sup>††</sup> The coefficient  $z_c$  depends on the time spent in the compacted state.

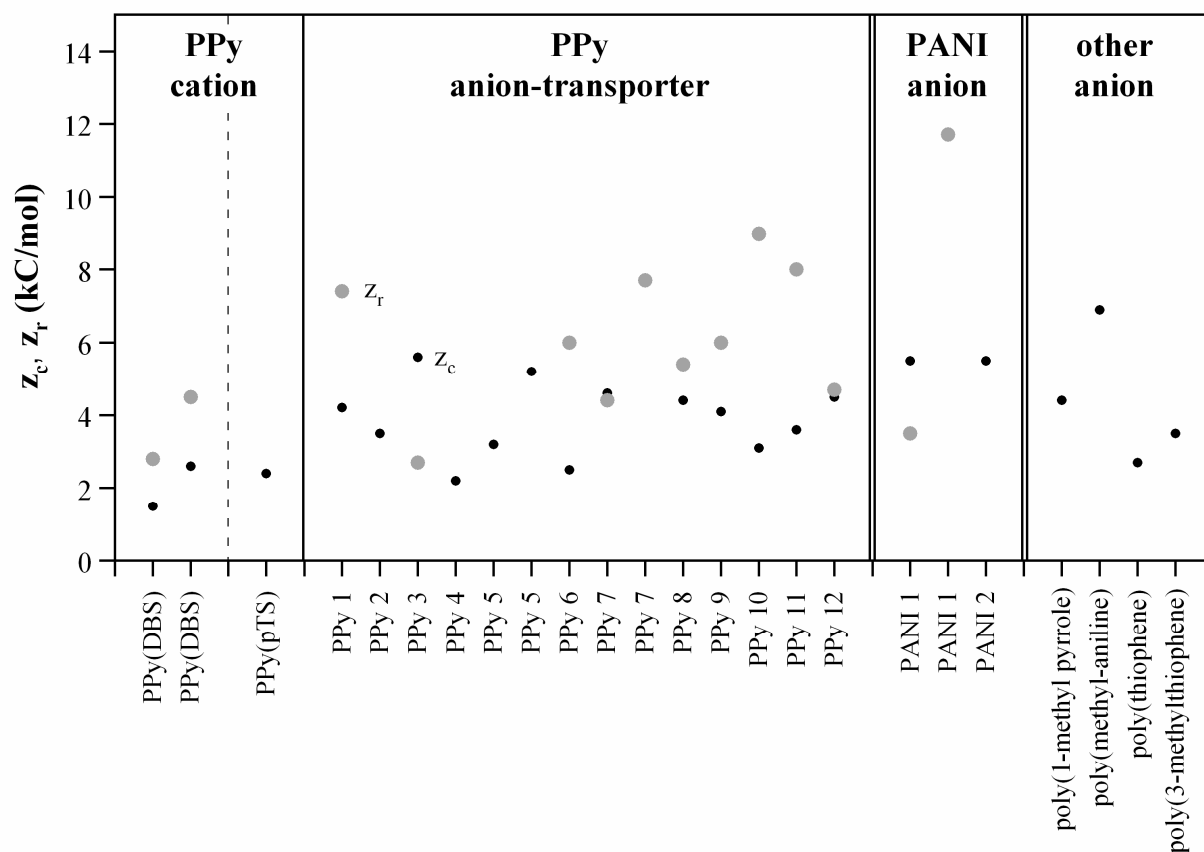


Figure 14-SI. Values of the conformational energies  $z_c$  (black dots) and  $z_r$  (gray dots) in various systems.

## REFERENCES

1. T. F. Otero, H. Grande, and J. Rodriguez, "Reinterpretation of Polypyrrole Electrochemistry after Consideration of Conformational Relaxation Processes," *J Phys Chem B*, 101, 3688-3697 (1997).
2. R. Kohlrausch, "Theorie des elektrischen Rückstandes in der Leidner Flasche," *Ann. Phys. Chem. (Poggendorff)*, 91, 56-82, 179-213 (1854).
3. A. Werner, "Quantitative Messungen der An- und Abklingung getrennter Phosphoreszenzbanden," *Annalen der Physik*, 329 (11), 164-190 (1907).
4. T. Förster, "Experimental and theoretical investigation of intermolecular transfer of electron activation energy," *Zeits. Naturforsch.*, 4a, 321 (1949).
5. X. Wang, Shapiro, Benjamin, Smela, Elisabeth, "Visualizing Ion Currents in Conjugated Polymers," *Advanced Materials*, 16 (18), 1605-1609 (2004).
6. X. Wang, B. Shapiro, and E. Smela, "Ion transport in conjugated polymers: Part 2. Modeling," in preparation (2006).

7. T. F. Otero and J. Padilla, "Anodic shrinking and compaction of polypyrrole blend: electrochemical reduction under conformational relaxation kinetic control," *J. Electroanal. Chem.*, 561, 167-171 (2004).
8. T. F. Otero, H. Grande, and J. Rodriguez, "Conformational relaxation during polypyrrole oxidation: from experiment to theory," *Electrochim. Acta*, 41 (11/12), 1863-1869 (1996).
9. T. F. Otero and I. Boyano, "Comparative Study of Conducting Polymers by the ESCR Model," *J. Phys. Chem. B*, 107, 6730-6738 (2003).
10. H. Grande, T. F. Otero, and I. Cantero, "Conformational relaxation in conducting polymers: effect of polymer-solvent interactions," *J. Non-Cryst. Solids*, 235, 619-622 (1998).
11. T. F. Otero, H. Grande, and J. Rodriguez, "Influence of the counterion size on the rate of electrochemical relaxation in polypyrrole," *Synth. Met.*, 83, 205 (1996).
12. H. Grande and T. F. Otero, "Conformational movements explain logarithmic relaxation in conducting polymers," *Electrochim. Acta*, 44, 1893-1900 (1999).
13. T. F. Otero and H. J. Grande, "Reversible 2D to 3D electrode transitions in polypyrrole films," *Colloid Surf. A*, 134 (1-2), 85-94 (1998).
14. T. F. Otero, H. Grande, and J. Rodriguez, "A new model for electrochemical oxidation of polypyrrole under conformational relaxation control," *J. Electroanal. Chem.*, 394, 211 (1995).
15. T. F. Otero and H. Grande, "Thermally enhanced conformational relaxation during electrochemical oxidation of polypyrrole," *Electroanal. Chem.*, 414, 171 (1996).
16. T. F. Otero, M. T. Cortes, and I. Boyano, "Molar enthalpy of the polypyrrole electrochemistry," *J. Electroanal. Chem.*, 562, 161-165 (2004).
17. T. F. Otero and I. Boyano, "Potentiostatic oxidation of polyaniline under conformational relaxation control: experimental and theoretical study," *J. Phys. Chem. B*, 107, 4269-4276 (2003).